Extending the VDPC+BCS formalism by including three-body forces*

Zi-Yu Xia (夏子育)†

Department of Physics, University of Shanghai for Science and Technology, Shanghai 200093, China

Abstract: Recently, Jia proposed a formalism to apply the variational principle to a coherent-pair condensate for a two-body Hamiltonian. The present study extends this formalism by including three-body forces. The result is the same as the so-called variation after particle-number projection in the BCS case, but now, the particle number is always conserved, and the time-consuming projection is avoided. Specifically, analytical formulas of the average energy are derived along with its gradient for a three-body Hamiltonian in terms of the coherent-pair structure. Gradient vanishment is required to obtain analytical expressions for the pair structure at the energy minimum. The new algorithm iterates on these pair-structure expressions to minimize energy for a three-body Hamiltonian. The new code is numerically demonstrated when applied to realistic two-body forces and random three-body forces in large model spaces. The average energy can be minimized to practically any arbitrary precision.

Keywords: three-body forces, BCS, variational principle applied directly to the coherent-pair condensate, variation after particle-number projection

DOI: 10.1088/1674-1137/acb14a

I. INTRODUCTION

Recently, Jia proposed a formalism [1, 2] to apply the variational principle directly to a coherent-pair condensate (VDPC) in the BCS case. The result is the same as the so-called variation after particle-number projection in the BCS case, but now, the particle number is always conserved, and the time-consuming projection is avoided. Refs. [1, 2] show that the VDPC+BCS algorithm easily computes with realistic interactions in large model spaces on a laptop. Currently, the VDPC+BCS formulas are derived under the assumption of a *two-body* Hamiltonian.

However, *three-body forces* sometimes play an important role in nuclear physics. Realistic nuclear-nuclear (*NN*) interactions were discovered by reproducing experimental *NN* phase shifts in microscopic many-body approaches. Nonrelativistic microscopic techniques based on realistic two-body *NN* interactions are widely known to miss the empirical saturation point of nuclear matter, demanding the use of three-body forces. Reproducing the experimental binding energies of light ($A = 3,\ 4$) nuclei needs three-body forces as well [3–8]. In recent years, various microscopic approaches, such as the Brueckner-Hartree-Fock (BHF) and extended BHF approaches [9–15], relativistic Dirac-BHF (DBHF) theory [16–23], in-medium *T*-matrix and Green function methods [24–35], and many-body variational approaches [36–41], have been used to investigate the equation of state (EOS) and single particle (s.p.) properties of asymmetric nuclear matter. To some extent, almost all microscopic methods are able to duplicate the empirical value of symmetry energy at the empirical saturation density. However, at large densities, the density dependence of symmetry energy anticipated by various methods and/or distinct NN interactions was found to be substantially different [42–44]. Moreover, when calculating the EOS of pure neutron matter, which is required for the estimation of critical parameters such as the symmetry energy and, in general, for the description of neutron-rich matter in neutron stars, the differences and uncertainties increase [45–49]. Neglecting three-body forces between nucleons in the dense medium is thought to be the cause of these deficits. Variational and BHF computations that take three-body forces into account produce a realistic description of cold nuclear matter, accurately matching the symmetric EOS saturation point [36, 37, 50–54].

This work extends the VDPC+BCS formalism by including three-body forces. Specifically, analytical formulas of the average energy were derived along with its gradient for a three-body Hamiltonian in terms of the coherent-pair structure v_α. Gradient vanishment was required to obtain analytical expressions for the pair structure v_α at the energy minimum. Asymptotic behaviors of v_α away from (above or below) the Fermi surface were

Received 15 June 2022; Accepted 9 January 2023; Published online 10 January 2023

* Supported by the National Natural Science Foundation of China (11405109)

† E-mail: 192262026@st.usst.edu.cn

examined. The new algorithm iterates on these v_α expressions to minimize energy for a three-body Hamiltonian. A computer code was developed (published together with this manuscript) to implement the algorithm. The new code is numerically demonstrated in application to realistic two-body forces and random three-body forces in large model spaces. The average energy can be minimized to practically any arbitrary precision. In the future, it is planned to use realistic three-body forces and study their effect on the coherent-pair condensate.

Previous studies closely related to this work can be pointed out. For instance, there are studies on the projection of BCS wave functions onto good particle numbers before [55–59] or after [60, 61] energy variation. Likewise, there are studies on the projection of HFB wavefunction (see Refs. [62–66] before such variation and Refs. [60, 61] after such variation). We can also mention the generalized seniority method [67–72], which breaks either BCS or HFB pairs to approximate the shell-model.

The paper is organized as follows. The formalism for the condensate of coherent pairs is revisited in Sec. II. The analytical equation for the average energy is derived in Sec. III. Then, the energy gradient as well as v_α at the energy minimum are derived, and the asymptotic behavior of v_α away from the Fermi surface is explored in Sec. IV. Section V describes the computer algorithm. In Section VI, the proposed algorithm is applied to a semirealistic example. Finally, this work is summarized in Sec. VII.

II. COHERENT-PAIR CONDENSATE

The formalism for the condensate of coherent pairs, whose state is zero generalized seniority [73], is briefly reviewed in this section. For simplicity, only one type of nucleus is considered. The time-reversal self-consistent symmetry [61, 74] is assumed in this work. The single-particle state $|\alpha\rangle$ is hypothesized to present Kramers degeneracy with its time-reversed partner $|\tilde{\alpha}\rangle$ ($|\tilde{\tilde{\alpha}}\rangle = -|\alpha\rangle$). No additional symmetries are postulated in this study other than the two previously mentioned.

The $2N$-particle system in ground state could be regarded as a condensate with N-pairs of particles,

$$|\phi_N\rangle = \frac{1}{\sqrt{\chi_N}}(P^\dagger)^N|0\rangle, \tag{1}$$

where

$$\chi_N = \langle 0|P^N(P^\dagger)^N|0\rangle \tag{2}$$

is the normalization. The coherent pair-creation operator is

$$P^\dagger = \frac{1}{2}\sum_\alpha v_\alpha a^\dagger_\alpha a^\dagger_{\tilde{\alpha}} = \sum_{\alpha\in\Theta} v_\alpha P^\dagger_\alpha, \tag{3}$$

where

$$P^\dagger_\alpha = a^\dagger_\alpha a^\dagger_{\tilde{\alpha}} = P^\dagger_{\tilde{\alpha}} \tag{4}$$

creates one pair of particles on $|\alpha\rangle$ and $|\tilde{\alpha}\rangle$orbits. In Eq. (3), Θ is a set that selects one from each of all degenerate pairs $|\alpha\rangle$ and $|\tilde{\alpha}\rangle$, respectively (for example, it only selects those single-particle levels with a positive magnetic quantum number m). In Eq. (3), the summation index α and $\alpha\in\Theta$ sum over single-particle and pair indices, respectively. The single-particle state $|\phi_N\rangle$ is time even by assumptions, which implies that the pair structure v_α (3) is real.

The many-pair density matrix is introduced in Refs. [67, 68] as

$$\begin{aligned} t^{[\gamma_1\gamma_2\ldots\gamma_r],N}_{\alpha_1\alpha_2\ldots\alpha_p;\beta_1\beta_2\ldots\beta_q} \equiv &\langle 0|P^{N-p}P_{\gamma_1}P_{\gamma_2}\ldots P_{\gamma_r} \\ &\times P_{\alpha_1}P_{\alpha_2}\ldots P_{\alpha_p}P^\dagger_{\beta_1}P^\dagger_{\beta_2}\ldots P^\dagger_{\beta_q} \\ &\times P^\dagger_{\gamma_1}P^\dagger_{\gamma_2}\ldots P^\dagger_{\gamma_r}(P^\dagger)^{N-q}|0\rangle. \end{aligned} \tag{5}$$

The pair indices $\alpha_1\alpha_2\ldots\alpha_p$, $\beta_1\beta_2\ldots\beta_q$, $\gamma_1\gamma_2\ldots\gamma_r$ are all distinct. Owing to the Pauli principle, if there are duplicated P operators, or duplicated $P^\dagger$ operators, Eq. (5) vanishes. Moreover, $\alpha_1\alpha_2\ldots\alpha_p$ and $\beta_1\beta_2\ldots\beta_q$ must have no common index (the common ones have been transferred to $\gamma_1\gamma_2\ldots\gamma_r$). Physically, $P_{\gamma_1}\ldots P_{\gamma_r}$ together with $P^\dagger_{\gamma_1}\ldots P^\dagger_{\gamma_r}$ Pauli block the $[\gamma_1\gamma_2\ldots\gamma_r]$ paired-orbitals from the space, which is explained as follows.

Reference [68] introduced Pauli-blocked normalizations as a special case of Eq. (5) when $p = q = 0$,

$$\begin{aligned} \chi^{[\gamma_1\gamma_2\ldots\gamma_r]}_N &\equiv t^{[\gamma_1\gamma_2\ldots\gamma_r],N}_{;} \\ &= \langle 0|P^N P_{\gamma_1}P_{\gamma_2}\ldots P_{\gamma_r}P^\dagger_{\gamma_1}P^\dagger_{\gamma_2}\ldots P^\dagger_{\gamma_r}(P^\dagger)^N|0\rangle. \end{aligned} \tag{6}$$

By substituting Eq. (3) into $(P^\dagger)^N$ and polynomially expanding, those terms with $P^\dagger_{\gamma_1}P^\dagger_{\gamma_2}\ldots P^\dagger_{\gamma_r}$ vanish owing to the Pauli principle. In other words, the $[P_{\gamma_1}P_{\gamma_2}\ldots P_{\gamma_r}]$ paired-orbitals are Pauli blocked. Ref. [68] provides the relationship between the many-pair density matrix (5) and the normalizations (6),

$$\begin{aligned} t^{[\gamma_1\gamma_2\ldots\gamma_r],M}_{\alpha_1\alpha_2\ldots\alpha_p;\beta_1\beta_2\ldots\beta_q} = &\frac{(M-p)!(M-q)!}{[(M-p-q)!]^2} \\ &\times v_{\alpha_1}v_{\alpha_2}\ldots v_{\alpha_p}v_{\beta_1}v_{\beta_2}\ldots v_{\beta_q} \\ &\times \chi^{[\alpha_1\alpha_2\ldots\alpha_p\beta_1\beta_2\ldots\beta_q\gamma_1\gamma_2\ldots\gamma_r]}_{M-p-q}. \end{aligned} \tag{7}$$

We could compute normalizations (2) and (6) using recursive relations [75],

$$\chi_N = N\sum_{\alpha\in\Theta}(v_\alpha)^2\chi_{N-1}^{[\alpha]}, \tag{8}$$

$$\chi_N - \chi_N^{[\alpha]} = N^2(v_\alpha)^2\chi_{N-1}^{[\alpha]}, \tag{9}$$

with initial values $\chi_0 = \chi_0^{[\alpha]} = \chi_0^{[\alpha\beta]} = \cdots = 1$. Given that $\chi_0^{[\alpha]}$ is known, χ_1 can be computed by Eq. (8), and then $\chi_1^{[\alpha]}$ by Eq. (9). Similarly, all χ_N and $\chi_N^{[\alpha]}$can be derived. It is crucial to note that if the β index is Pauli-blocked ($P_\beta \neq P_\alpha$) according to Eqs. (8) and (9), they are still valid, and $\chi_N^{[\alpha\beta]}$ can be obtained. Similarly, $\chi_N^{[\alpha\beta\gamma]}$ can be easily obtained by Pauli blocking indices β and γ from the very beginning, and $\chi_N^{[\alpha\beta\gamma\mu]}$ by Pauli blocking β, γ, and μ. To increase the computation speed, a simpler formula was used to compute $\chi_N^{[\alpha\beta]}$ ($P_\alpha \neq P_\beta$):

$$(v_\alpha)^2\chi_N^{[\alpha]} - (v_\beta)^2\chi_N^{[\beta]} = [(v_\alpha)^2 - (v_\beta)^2]\chi_N^{[\alpha\beta]}, \tag{10}$$

Note that if the γ (or γ together with μ) index is Pauli-blocked according to Eq. (10), it is still valid.

To provide a physical explanation, the relationship between the average occupation number and the normalizations is expressed as follows:

$$n_\alpha = \langle\phi_N|\hat{n}_\alpha|\phi_N\rangle = 1 - \frac{\chi_N^{[\alpha]}}{\chi_N}, \tag{11}$$

where

$$\hat{n}_\alpha = a_\alpha^\dagger a_\alpha. \tag{12}$$

Equation (11) is valid if the β index is Pauli-blocked ($P_\beta \neq P_\alpha$)

$$\langle\phi_N^{[\beta]}|\hat{n}_\alpha|\phi_N^{[\beta]}\rangle = 1 - \frac{\chi_N^{[\alpha\beta]}}{\chi_N^{[\beta]}}, \tag{13}$$

where

$$|\phi_N^{[\beta]}\rangle \equiv \frac{1}{\sqrt{\chi_N^{[\beta]}}}(P^\dagger - v_\beta P_\beta^\dagger)^N|0\rangle \tag{14}$$

is the pair condensate with β and $\tilde{\beta}$ blocked.

III. AVERAGE ENERGY

The antisymmetrized three-body Hamiltonian is

$$H = \sum_{\alpha\beta}\epsilon_{\alpha\beta}a_\alpha^\dagger a_\beta + \frac{1}{4}\sum_{\alpha\beta\gamma\mu}V_{\alpha\beta\gamma\mu}a_\alpha^\dagger a_\beta^\dagger a_\gamma a_\mu + \frac{1}{36}\sum_{\alpha\beta\gamma\mu\eta\zeta}W_{\alpha\beta\gamma\mu\eta\zeta}a_\alpha^\dagger a_\beta^\dagger a_\gamma^\dagger a_\mu a_\eta a_\zeta. \tag{15}$$

According to the ordering of $\alpha\beta\gamma\mu\eta\zeta$, one could obtain $V_{\alpha\beta\gamma\mu} = -\langle\alpha\beta|V|\gamma\mu\rangle$ and $W_{\alpha\beta\gamma\mu\eta\zeta} = -\langle\alpha\beta\gamma|W|\mu\eta\zeta\rangle$. H is assumed to be time-even ($\epsilon_{\alpha\beta} = \epsilon_{\tilde{\beta}\tilde{\alpha}}$, $V_{\alpha\beta\gamma\mu} = V_{\tilde{\mu}\tilde{\gamma}\tilde{\beta}\tilde{\alpha}}$, $W_{\alpha\beta\gamma\mu\eta\zeta} = W_{\tilde{\zeta}\tilde{\eta}\tilde{\mu}\tilde{\gamma}\tilde{\beta}\tilde{\alpha}}$) and $\epsilon_{\alpha\beta}$, $V_{\alpha\beta\gamma\mu}$, $W_{\alpha\beta\gamma\mu\eta\zeta}$ are assumed to be real. There is no additional assumption.

Given that the one-body and two-body parts of the average energy were already derived in the original VDPC+BCS algorithm, in this study the three-body part of the average energy $\overline{W} = \langle\phi_N|\hat{W}|\phi_N\rangle$ is described in the canonical basis (3), where $\hat{W} = \frac{1}{36}\sum_{\alpha\beta\gamma\mu\eta\zeta}W_{\alpha\beta\gamma\mu\eta\zeta}a_\alpha^\dagger a_\beta^\dagger a_\gamma^\dagger a_\mu a_\eta a_\zeta$. Only three types contribute to the three-body part of the average energy $\hat{W}$ ($P_\alpha \neq P_\beta$, $P_\alpha \neq P_\gamma$ and $P_\beta \neq P_\gamma$):

$$\underbrace{a_\beta^\dagger \overbrace{a_\alpha^\dagger a_{\tilde{\alpha}}^\dagger}^{P_\alpha^\dagger}}_{\texttt{common}}\underbrace{\overbrace{a_{\tilde{\alpha}}a_\alpha}^{P_\alpha}}_{\texttt{common}}\underbrace{a_\beta}_{\texttt{common}},\ \underbrace{a_\gamma^\dagger}_{\texttt{common}}\underbrace{\overbrace{a_\alpha^\dagger a_{\tilde{\alpha}}^\dagger}^{P_\alpha^\dagger}\overbrace{a_{\tilde{\beta}}a_\beta}^{P_\beta}}_{\texttt{different}}\underbrace{a_\gamma}_{\texttt{common}},\ \text{and}\ \underbrace{a_\alpha^\dagger a_\beta^\dagger}_{\texttt{common}}\underbrace{a_\gamma^\dagger a_\gamma}_{\texttt{common}}.$$

The term "common" means that the creation and annihilation operators have common indices. There are only three types because indices α, β, γ and μ, η, ζ must differ in time-reversed pairs [67].

The first type is

$$\begin{aligned}\text{type 1} &= \langle 0|P^N a_\beta^\dagger a_\alpha^\dagger a_{\tilde{\alpha}}^\dagger a_{\tilde{\alpha}}a_\alpha a_\beta (P^\dagger)^N|0\rangle \\ &= \langle 0|P^N a_\beta^\dagger a_\alpha^\dagger a_\alpha a_\beta (P^\dagger)^N|0\rangle \\ &= \chi_N - \chi_N^{[\alpha]} - \chi_N^{[\beta]} + \chi_N^{[\alpha\beta]}.\end{aligned} \tag{16}$$

In the first step, $P_\alpha^\dagger$ creates $|\alpha\rangle$ and $|\tilde{\alpha}\rangle$ simultaneously, which could be derived from Eq. (4). Therefore, $|\alpha\rangle$ and $|\tilde{\alpha}\rangle$ are either both occupied or both empty in $(P^\dagger)^N|0\rangle$. As a result, $a_\alpha^\dagger a_{\tilde{\alpha}}^\dagger a_{\tilde{\alpha}}a_\alpha(P^\dagger)^N|0\rangle = a_\alpha^\dagger a_\alpha a_{\tilde{\alpha}}^\dagger a_{\tilde{\alpha}}(P^\dagger)^N|0\rangle = \hat{n}_\alpha\hat{n}_{\tilde{\alpha}}(P^\dagger)^N|0\rangle = \hat{n}_\alpha(P^\dagger)^N|0\rangle = a_\alpha^\dagger a_\alpha(P^\dagger)^N|0\rangle$. The second step uses $a_\beta^\dagger a_\alpha^\dagger a_\alpha a_\beta = 1 - a_\alpha a_\alpha^\dagger - a_\beta a_\beta^\dagger + a_\beta a_\alpha a_\alpha^\dagger a_\beta^\dagger$, which could be derived by basic anticommutation relation. Thus, using definition (6), one could derive the result. Eq. (16) can also be derived by directly exchanging the order of creation and annihilation operators using the basic anticommutation relation from the very beginning, and eventually, by combining terms, it can be simplified to Eq. (16). Using Eq. (9) and$\chi_N^\beta - \chi_N^{[\alpha\beta]} = N^2(v_\alpha)^2\chi_{N-1}^{[\alpha\beta]}$ [Pauli blocking the β index ($P_\beta \neq P_\alpha$) in Eq. (9)], and factorizing out $N^2(v_\alpha)^2$, the following expression is obtained:

$$\text{type 1} = N^2(v_\alpha)^2\left(\chi_{N-1}^{[\alpha]} - \chi_{N-1}^{[\alpha\beta]}\right).$$

Then, by using $\chi_{N-1}^{[\alpha]} - \chi_{N-1}^{[\alpha\beta]} = (N-1)^2(v_\beta)^2\chi_{N-2}^{[\alpha\beta]}$ [Pauli

blocking the β index ($P_\beta \neq P_\alpha$), replacing N by $N-1$, and exchanging α and β in Eq. (9)], the final expression is derived:

$$\text{type 1} = N^2(N-1)^2(v_\alpha v_\beta)^2\chi_{N-2}^{[\alpha\beta]}. \tag{17}$$

The second type satisfies $a_\gamma^\dagger a_\alpha^\dagger a_{\tilde{\alpha}}^\dagger a_{\tilde{\beta}} a_\beta a_\gamma = a_\gamma^\dagger P_\alpha^\dagger P_\beta a_\gamma = P_\beta P_\alpha^\dagger - a_\gamma P_\beta P_\alpha^\dagger a_\gamma^\dagger$ according to the basic anticommutation relation. Equations (5), (7), and (9) imply

$$\begin{aligned}\text{type 2} &= \langle 0|P^N a_\gamma^\dagger a_\alpha^\dagger a_{\tilde{\alpha}}^\dagger a_{\tilde{\beta}} a_\beta a_\gamma (P^\dagger)^N|0\rangle = t_{\beta;\alpha}^{N+1} - t_{\beta;\alpha}^{[\gamma],N+1} \\ &= N^2 v_\alpha v_\beta \chi_{N-1}^{[\alpha\beta]} - N^2 v_\alpha v_\beta \chi_{N-1}^{[\alpha\beta\gamma]} \\ &= N^2(N-1)^2 v_\alpha v_\beta (v_\gamma)^2 \chi_{N-2}^{[\alpha\beta\gamma]}. \end{aligned} \tag{18}$$

The third type satisfies $a_\alpha^\dagger a_\beta^\dagger a_\gamma^\dagger a_\gamma a_\beta a_\alpha = 1 - a_\alpha a_\alpha^\dagger - s a_\beta a_\beta^\dagger - a_\gamma a_\gamma^\dagger + a_\alpha a_\beta a_\beta^\dagger a_\alpha^\dagger + a_\alpha a_\gamma a_\gamma^\dagger a_\alpha^\dagger + a_\beta a_\gamma a_\gamma^\dagger a_\beta^\dagger - a_\alpha a_\beta a_\gamma a_\gamma^\dagger a_\beta^\dagger a_\alpha^\dagger$ according to the basic anticommutation relation. Thus, definition (6) implies

$$\begin{aligned}\text{type 3} &= \langle 0|P^N a_\alpha^\dagger a_\beta^\dagger a_\gamma^\dagger a_\gamma a_\beta a_\alpha (P^\dagger)^N|0\rangle \\ &= \chi_N - \chi_N^{[\alpha]} - \chi_N^{[\beta]} + \chi_N^{[\alpha\beta]} - \chi_N^{[\gamma]} + \chi_N^{[\alpha\gamma]} + \chi_N^{[\beta\gamma]} - \chi_N^{[\alpha\beta\gamma]} \\ &= N^2(N-1)^2(v_\alpha v_\beta)^2 \chi_{N-2}^{[\alpha\beta]} - N^2(N-1)^2(v_\alpha v_\beta)^2 \chi_{N-2}^{[\alpha\beta\gamma]} \\ &= N^2(N-1)^2(N-2)^2(v_\alpha v_\beta v_\gamma)^2 \chi_{N-3}^{[\alpha\beta\gamma]}. \end{aligned} \tag{19}$$

The expectation value of $\hat{W}$ is

$$\begin{aligned}\langle\phi_N|\hat{W}|\phi_N\rangle = &\sum_{\alpha,\beta\in\Theta}^{P_\alpha\neq P_\beta} 2V_{\beta\alpha\tilde{\alpha}\tilde{\alpha}\alpha\beta}\langle\phi_N|a_\beta^\dagger a_\alpha^\dagger a_{\tilde{\alpha}}^\dagger a_{\tilde{\alpha}} a_\alpha a_\beta|\phi_N\rangle \\ &+ \sum_{\alpha,\beta,\gamma\in\Theta}^{\boldsymbol{dif}\,\alpha\beta\gamma} 2V_{\gamma\alpha\tilde{\beta}\tilde{\beta}\gamma}\langle\phi_N|a_\gamma^\dagger a_\alpha^\dagger a_{\tilde{\alpha}}^\dagger a_{\tilde{\beta}} a_\beta a_\gamma|\phi_N\rangle \\ &+ \sum_{\alpha,\beta,\gamma\in\Theta}^{\boldsymbol{dif}\,\alpha\beta\gamma} (\frac{1}{3}V_{\alpha\beta\gamma\gamma\beta\alpha} + V_{\tilde{\alpha}\beta\gamma\gamma\beta\tilde{\alpha}}) \\ &\times\langle\phi_N|a_\alpha^\dagger a_\beta^\dagger a_\gamma^\dagger a_\gamma a_\beta a_\alpha|\phi_N\rangle. \end{aligned} \tag{20}$$

The term "$\boldsymbol{dif}\,\alpha\beta\gamma$" means $P_\alpha \neq P_\beta$, $P_\alpha \neq P_\gamma$, and $P_\beta \neq P_\gamma$(no two are the same). The first term of Eq. (20) collects 72 equal contributions, which not only cancels the factor 1/36 in $\hat{W}$ but also yields the factor 2. These 72 equal contributions are further explained next. It is not too difficult to find $V_{\beta\alpha\tilde{\alpha}\tilde{\alpha}\alpha\beta} = -V_{\beta\alpha\tilde{\alpha}\tilde{\alpha}\beta\alpha}$ and $a_\beta^\dagger a_\alpha^\dagger a_{\tilde{\alpha}}^\dagger a_{\tilde{\alpha}} a_\alpha a_\beta = -a_\beta^\dagger a_\alpha^\dagger a_{\tilde{\alpha}}^\dagger a_{\tilde{\alpha}} a_\beta a_\alpha$. Then, the following expression is obtained: $\sum_{\alpha,\beta\in\Theta}^{P_\alpha\neq P_\beta} \frac{1}{36} V_{\beta\alpha\tilde{\alpha}\tilde{\alpha}\alpha\beta}\langle\phi_N|a_\beta^\dagger a_\alpha^\dagger a_{\tilde{\alpha}}^\dagger a_{\tilde{\alpha}} a_\alpha a_\beta|\phi_N\rangle = \sum_{\alpha,\beta\in\Theta}^{P_\alpha\neq P_\beta} \frac{1}{36} V_{\beta\alpha\tilde{\alpha}\tilde{\alpha}\beta\alpha}\langle\phi_N|a_\beta^\dagger a_\alpha^\dagger a_{\tilde{\alpha}}^\dagger a_{\tilde{\alpha}} a_\beta a_\alpha|\phi_N\rangle$. Each term in these two summations is distinct because they do not follow the same order, as in $21\bar{1}\bar{1}12 \neq 21\bar{1}\bar{1}21$. Thus, in terms of the last 3 indices, any permutation of the set $\{\tilde{\alpha}, \alpha, \beta\}$ contributes. Besides, based on the time-even assumption introduced before, the following expression is obtained: $V_{\beta\alpha\tilde{\alpha}\tilde{\alpha}\alpha\beta} = V_{\tilde{\beta}\tilde{\alpha}\alpha\alpha\tilde{\alpha}\tilde{\beta}}$. Given that $a_\alpha^\dagger(P^\dagger)^N|0\rangle = a_{\tilde{\alpha}}^\dagger(P^\dagger)^N|0\rangle$ (both block the pair indices α from $(P^\dagger)^N|0\rangle$), it is obtained that $\langle\phi_N|a_\beta^\dagger a_\alpha^\dagger a_{\tilde{\alpha}}^\dagger a_{\tilde{\alpha}} a_\alpha a_\beta|\phi_N\rangle = \langle\phi_N|a_{\tilde{\beta}}^\dagger a_{\tilde{\alpha}}^\dagger a_\alpha^\dagger a_\alpha a_{\tilde{\alpha}} a_{\tilde{\beta}}|\phi_N\rangle$. In conclusion, all orderings of the permutations that contribute are

$$\underbrace{\beta\,\alpha\,\tilde{\alpha}}_{\mathcal{P}\{\alpha\tilde{\alpha}\beta\}}\underbrace{\tilde{\alpha}\,\alpha\,\beta}_{\mathcal{P}\{\alpha\tilde{\alpha}\beta\}} \quad + \quad \underbrace{\tilde{\beta}\,\tilde{\alpha}\,\alpha}_{\mathcal{P}\{\alpha\tilde{\alpha}\tilde{\beta}\}}\underbrace{\alpha\,\tilde{\alpha}\,\tilde{\beta}}_{\mathcal{P}\{\alpha\tilde{\alpha}\tilde{\beta}\}}.$$

The symbol $\mathcal{P}\{\alpha\tilde{\alpha}\beta\}$ denotes all permutations of the set $\{\alpha, \tilde{\alpha}, \beta\}$. Thus, the total number of permutations that contribute are $\mathrm{P}_3^3 \times \mathrm{P}_3^3 + \mathrm{P}_3^3 \times \mathrm{P}_3^3 = 2 \times \mathrm{P}_3^3 \times \mathrm{P}_3^3 = 72$, where $\mathrm{P}_3^3 = 3!$ is the number of permutations. The second term of Eq. (20) collects 72 equal contributions as well, which are

$$\underbrace{\gamma\,\alpha\,\tilde{\alpha}}_{\mathcal{P}\{\alpha\tilde{\alpha}\gamma\}}\underbrace{\tilde{\beta}\,\beta\,\gamma}_{\mathcal{P}\{\beta\tilde{\beta}\gamma\}} \quad + \quad \underbrace{\tilde{\gamma}\,\tilde{\alpha}\,\alpha}_{\mathcal{P}\{\alpha\tilde{\alpha}\tilde{\gamma}\}}\underbrace{\beta\,\tilde{\beta}\,\tilde{\gamma}}_{\mathcal{P}\{\beta\tilde{\beta}\tilde{\gamma}\}}.$$

The third term is slightly more complicated and will be thoroughly described next.

The expressions $V_{\alpha\beta\gamma\gamma\beta\alpha} = V_{\tilde{\alpha}\tilde{\beta}\tilde{\gamma}\tilde{\gamma}\tilde{\beta}\tilde{\alpha}}$ and $V_{\tilde{\alpha}\beta\gamma\gamma\beta\tilde{\alpha}} = V_{\alpha\tilde{\beta}\tilde{\gamma}\tilde{\gamma}\tilde{\beta}\alpha}$ have already been derived. However, in general, $V_{\alpha\beta\gamma\gamma\beta\alpha}$ is not equal to $V_{\tilde{\alpha}\beta\gamma\gamma\beta\tilde{\alpha}}$. Therefore, the discussion is split into two cases: no tilde and two tildes. In the case "no tilde", $V_{\alpha\beta\gamma\gamma\beta\alpha} = -V_{\alpha\beta\gamma\gamma\alpha\beta} = V_{\alpha\beta\gamma\beta\alpha\gamma} = -V_{\alpha\beta\gamma\beta\gamma\alpha} = V_{\alpha\beta\gamma\alpha\gamma\beta} = -V_{\alpha\beta\gamma\alpha\beta\gamma}$; only these 6 permutations contribute. If other orderings of the first three indices and last three indices are set, such as $V_{\beta\alpha\gamma\gamma\beta\alpha}$, then indices α and β are exchanged (they are both subscripts of the summation, belong to the same space, and are commutative), leading to $V_{\alpha\beta\gamma\gamma\alpha\beta}$, i.e., one of the six previous permutations. Evidently, these six permutations have their time-reversed partner, i.e., $V_{\tilde{\alpha}\tilde{\beta}\tilde{\gamma}\tilde{\gamma}\tilde{\beta}\tilde{\alpha}} = -V_{\tilde{\alpha}\tilde{\beta}\tilde{\gamma}\tilde{\gamma}\alpha\tilde{\beta}} = V_{\tilde{\alpha}\tilde{\beta}\tilde{\gamma}\tilde{\beta}\tilde{\alpha}\tilde{\gamma}} = -V_{\tilde{\alpha}\tilde{\beta}\tilde{\gamma}\tilde{\beta}\tilde{\gamma}\tilde{\alpha}} = V_{\tilde{\alpha}\tilde{\beta}\tilde{\gamma}\tilde{\alpha}\tilde{\gamma}\tilde{\beta}} = -V_{\tilde{\alpha}\tilde{\beta}\tilde{\gamma}\tilde{\alpha}\tilde{\beta}\tilde{\gamma}}$, so there are $2 \times 6 = 12$ in total, which makes the factor 1/3. There is an alternative formula to calculate this number, $72 \div 6 = 12$. If α, β, and γ are assumed not to be commutative, there are 72 permutations. However, because they are commutative, we need to divide by P_3^3, which is the number of all permutations of $\{\alpha, \beta, \gamma\}$. In the case "two tildes", given that there are 2 commutative indices β and γ, the total number of the permutations that contribute are $72 \div \mathrm{P}_2^2 = 36$, which cancels the factor $\frac{1}{36}$.

Substituting Eqs. (17), (18), and (19) into Eq. (20), the following expression is obtained:

$$\langle\phi_N|\hat{W}|\phi_N\rangle = \frac{N^2(N-1)^2}{\chi_N}\Bigg(\sum_{\alpha,\beta\in\Theta}^{P_\alpha\neq P_\beta} G_{\alpha\alpha,\beta}(v_\alpha v_\beta)^2\chi_{N-2}^{[\alpha\beta]} + \sum_{\alpha,\beta,\gamma\in\Theta}^{\boldsymbol{dif}\,\alpha\beta\gamma} G_{\alpha\beta,\gamma}v_\alpha v_\beta(v_\gamma)^2\chi_{N-2}^{[\alpha\beta\gamma]} + \frac{(N-2)^2}{3}\sum_{\alpha,\beta,\gamma\in\Theta}^{\boldsymbol{dif}\,\alpha\beta\gamma} F_{\alpha\beta\gamma}(v_\alpha v_\beta v_\gamma)^2\chi_{N-3}^{[\alpha\beta\gamma]}\Bigg), \quad (21)$$

where

$$G_{\alpha\beta,\gamma} = V_{\gamma\alpha\tilde{\alpha}\tilde{\beta}\beta\gamma} + V_{\tilde{\gamma}\alpha\tilde{\alpha}\tilde{\beta}\beta\tilde{\gamma}} = 2V_{\gamma\alpha\tilde{\alpha}\tilde{\beta}\beta\gamma}, \quad (22)$$

$$F_{\alpha\beta\gamma} = V_{\alpha\beta\gamma\gamma\beta\alpha} + V_{\tilde{\alpha}\beta\gamma\gamma\beta\tilde{\alpha}} + V_{\alpha\tilde{\beta}\gamma\gamma\tilde{\beta}\alpha} + V_{\alpha\beta\tilde{\gamma}\tilde{\gamma}\beta\alpha}. \quad (23)$$

Note that $G_{\alpha\beta,\gamma} = G_{\beta\alpha,\gamma} = G_{\tilde{\alpha}\beta,\gamma} = G_{\alpha\beta,\tilde{\gamma}}$, $F_{\alpha\beta\gamma} = F_{\mathcal{P}\{\alpha\beta\gamma\}} = F_{\tilde{\alpha}\beta\gamma}$, $G_{\alpha\alpha,\gamma} = F_{\alpha\alpha\gamma}$, $G_{\alpha\beta,\alpha} = G_{\alpha\beta,\beta} = F_{\alpha\alpha\alpha} = 0$, and $\sum_{\alpha,\beta,\gamma\in\Theta}^{\boldsymbol{dif}\,\alpha\beta\gamma} V_{\tilde{\alpha}\beta\gamma\gamma\beta\tilde{\alpha}} = \sum_{\alpha,\beta,\gamma\in\Theta}^{\boldsymbol{dif}\,\alpha\beta\gamma} V_{\alpha\tilde{\beta}\gamma\gamma\tilde{\beta}\alpha} = \sum_{\alpha,\beta,\gamma\in\Theta}^{\boldsymbol{dif}\,\alpha\beta\gamma} V_{\alpha\beta\tilde{\gamma}\tilde{\gamma}\beta\alpha}$.

By appending the three-body result (21) to the two-body expression, which is Eq. (25) of Ref. [1], the following average energy is obtained:

$$\langle\phi_N|H|\phi_N\rangle = \frac{N^2}{\chi_N}\Bigg[\sum_{\alpha\in\Theta}(2\epsilon_{\alpha\alpha}+G_{\alpha\alpha})(v_\alpha)^2\chi_{N-1}^{[\alpha]} + \sum_{\alpha,\beta\in\Theta}^{P_\alpha\neq P_\beta} G_{\alpha\beta}v_\alpha v_\beta\chi_{N-1}^{[\alpha\beta]} + (N-1)^2\Bigg(\sum_{\alpha,\beta\in\Theta}^{P_\alpha\neq P_\beta}\Lambda_{\alpha\beta}(v_\alpha v_\beta)^2\chi_{N-2}^{[\alpha\beta]} + \sum_{\alpha,\beta\in\Theta}^{P_\alpha\neq P_\beta} G_{\alpha\alpha,\beta}(v_\alpha v_\beta)^2\chi_{N-2}^{[\alpha\beta]} + \sum_{\alpha,\beta,\gamma\in\Theta}^{\boldsymbol{dif}\,\alpha\beta\gamma} G_{\alpha\beta,\gamma}v_\alpha v_\beta(v_\gamma)^2\chi_{N-2}^{[\alpha\beta\gamma]} + \frac{(N-2)^2}{3}\sum_{\alpha,\beta,\gamma\in\Theta}^{\boldsymbol{dif}\,\alpha\beta\gamma} F_{\alpha\beta\gamma}(v_\alpha v_\beta v_\gamma)^2\chi_{N-3}^{[\alpha\beta\gamma]}\Bigg)\Bigg], \quad (24)$$

where

$$G_{\alpha\beta} = V_{\alpha\tilde{\alpha}\tilde{\beta}\beta}, \quad (25)$$

$$\Lambda_{\alpha\beta} = V_{\alpha\beta\beta\alpha} + V_{\alpha\tilde{\beta}\tilde{\beta}\alpha}. \quad (26)$$

The average energy is expressed by normalizations in Eq. (24), which is used in coding.

For a physical explanation, another equivalent expression can be obtained based on occupation numbers. Taking Eqs. (9) and (11) into (21), the following equation is obtained:

$$\langle\phi_N|\hat{W}|\phi_N\rangle = \sum_{\alpha,\beta\in\Theta}^{P_\alpha\neq P_\beta} G_{\alpha\alpha,\beta}\langle\phi_N|\hat{n}_\alpha|\phi_N\rangle\langle\phi_{N-1}^{[\alpha]}|\hat{n}_\beta|\phi_{N-1}^{[\alpha]}\rangle + \sum_{\alpha,\beta,\gamma\in\Theta}^{\boldsymbol{dif}\,\alpha\beta\gamma} G_{\alpha\beta,\gamma}\frac{v_\alpha}{v_\beta}(1-\langle\phi_N|\hat{n}_\alpha|\phi_N\rangle) \times\langle\phi_N^{[\alpha]}|\hat{n}_\beta|\phi_N^{[\alpha]}\rangle\langle\phi_{N-1}^{[\alpha\beta]}|\hat{n}_\gamma|\phi_{N-1}^{[\alpha\beta]}\rangle + \frac{1}{3}\sum_{\alpha,\beta,\gamma\in\Theta}^{\boldsymbol{dif}\,\alpha\beta\gamma} F_{\alpha\beta\gamma}\langle\phi_N|\hat{n}_\alpha|\phi_N\rangle\langle\phi_{N-1}^{[\alpha]}|\hat{n}_\beta|\phi_{N-1}^{[\alpha]}\rangle \times\langle\phi_{N-2}^{[\alpha\beta]}|\hat{n}_\gamma|\phi_{N-2}^{[\alpha\beta]}\rangle. \quad (27)$$

IV. GRADIENT OF ENERGY

The average energy gradient expressed by the pair structure v_α (3) is derived in this section. In addition, the analytical formula v_α at energy minimum is presented. Finally, the asymptotic behavior of v_α away from (above or below) the Fermi surface is described.

Equation (21) expresses the three-body part $\overline{W}$ of the average energy in terms of (Pauli-blocked) normalizations χ_N. To derive the gradient of $\overline{W}$, the gradient of χ_N is first introduced. Under infinitesimal change of v_α, δv_α, the variation of χ_N [1] is

$$\delta\chi_N = \frac{2}{v_\alpha}(\chi_N - \chi_N^{[\alpha]})\delta v_\alpha \quad (28a)$$

$$= 2N^2 v_\alpha\chi_{N-1}^{[\alpha]}\delta v_\alpha. \quad (28b)$$

The last step uses Eq. (9).

If the β index ($P_\beta \neq P_\alpha$) is Pauli blocked in Eqs. (28a) and (28b) from the very beginning, the derivation remains valid, so $\delta\chi_N^{[\beta]}$ can be obtained. Note that $\delta\chi_N^{[\alpha]}/\delta v_\alpha = 0$. Similarly, $\delta\chi_N^{[\beta\gamma]}$ could be easily obtained by Pauli blocking indices β and γ from the very beginning and $\delta\chi_N^{[\beta\gamma\mu]}$ by Pauli blocking β, γ, and μ. Substituting $\delta\chi_N$ (28a), $\delta\chi_N^{[\beta\gamma]}$, and $\delta\chi_N^{[\beta\gamma\mu]}$ into Eq. (21), applying simple calculus, and then collecting similar terms, the energy gradient is obtained:

$$\frac{\partial\overline{W}}{\partial v_\alpha}=\frac{\partial\left(\langle\phi_N|\hat{W}|\phi_N\rangle\right)}{\partial v_\alpha}$$
$$=-\frac{2N^2(N-1)^2}{\chi_N}\Bigg[\sum_{\beta,\gamma\in\Theta}^{\boldsymbol{dif}\,\alpha\beta\gamma}G_{\alpha\beta,\gamma}v_\beta(v_\gamma)^2\chi_{N-2}^{[\alpha\beta\gamma]}$$
$$+\frac{\chi_N^{[\alpha]}}{N^2(N-1)^2v_\alpha}\left(\langle\phi_N^{[\alpha]}|\hat{W}|\phi_N^{[\alpha]}\rangle-\overline{W}\right)\Bigg]. \tag{29a}$$

It is necessary to derive an equivalent expression to Eq. (29a) by substituting another form of $\delta\chi_N$, i.e., Eq. (28b), into Eq. (21),

$$\frac{\partial\overline{W}}{\partial v_\alpha}=\frac{2N^2}{\chi_N}\Bigg[(N-1)^2\sum_{\beta,\gamma\in\Theta}^{\boldsymbol{dif}\,\alpha\beta\gamma}G_{\alpha\beta,\gamma}v_\beta(v_\gamma)^2\chi_{N-2}^{[\alpha\beta\gamma]}$$
$$+v_\alpha\chi_{N-1}^{[\alpha]}\left(f_\alpha+\langle\phi_{N-1}^{[\alpha]}|\hat{W}|\phi_{N-1}^{[\alpha]}\rangle-\overline{W}\right)\Bigg], \tag{29b}$$

where

$$f_\alpha=(N-1)^2\sum_{\beta\in\Theta}^{P_\beta\neq P_\alpha}\left(G_{\alpha\alpha,\beta}+G_{\beta\beta,\alpha}\right)(v_\beta)^2\frac{\chi_{N-2}^{[\alpha\beta]}}{\chi_{N-1}^{[\alpha]}}$$
$$+(N-1)^2(N-2)^2\sum_{\beta,\gamma\in\Theta}^{\boldsymbol{dif}\,\alpha\beta\gamma}F_{\alpha\beta\gamma}(v_\beta v_\gamma)^2\frac{\chi_{N-3}^{[\alpha\beta\gamma]}}{\chi_{N-1}^{[\alpha]}}$$
$$+(N-1)^2\sum_{\beta,\gamma\in\Theta}^{\boldsymbol{dif}\,\alpha\beta\gamma}G_{\beta\gamma,\alpha}v_\beta v_\gamma\frac{\chi_{N-2}^{[\alpha\beta\gamma]}}{\chi_{N-1}^{[\alpha]}} \tag{30}$$

$$=\sum_{\beta\in\Theta}^{P_\beta\neq P_\alpha}\left(G_{\alpha\alpha,\beta}+G_{\beta\beta,\alpha}\right)\langle\phi_{N-1}^{[\alpha]}|\hat{n}_\beta|\phi_{N-1}^{[\alpha]}\rangle$$
$$+\sum_{\beta,\gamma\in\Theta}^{\boldsymbol{dif}\,\alpha\beta\gamma}F_{\alpha\beta\gamma}\langle\phi_{N-1}^{[\alpha]}|\hat{n}_\beta|\phi_{N-1}^{[\alpha]}\rangle\langle\phi_{N-2}^{[\alpha\beta]}|\hat{n}_\gamma|\phi_{N-2}^{[\alpha\beta]}\rangle$$
$$+\sum_{\beta,\gamma\in\Theta}^{\boldsymbol{dif}\,\alpha\beta\gamma}G_{\beta\gamma,\alpha}\frac{v_\gamma}{v_\beta}\langle\phi_{N-1}^{[\alpha]}|\hat{n}_\beta|\phi_{N-1}^{[\alpha]}\rangle(1-\langle\phi_{N-2}^{[\alpha\beta]}|\hat{n}_\gamma|\phi_{N-2}^{[\alpha\beta]}\rangle). \tag{31}$$

f_α is the three-body part of single-pair energy, similar to the three-body part of common HF single-particle energy.

By appending the three-body results (29a) and (29b) to the two-body expressions, which are Eqs. (31) and (32) of Ref. [1], the average energy gradient is obtained:

$$\frac{\partial\overline{E}}{\partial v_\alpha}=-\frac{2}{\chi_N}\Bigg[N^2\sum_{\beta\in\Theta}^{P_\beta\neq P_\alpha}G_{\alpha\beta}v_\beta\chi_{N-1}^{[\alpha\beta]}$$
$$+N^2(N-1)^2\sum_{\beta,\gamma\in\Theta}^{\boldsymbol{dif}\,\alpha\beta\gamma}G_{\alpha\beta,\gamma}v_\beta(v_\gamma)^2\chi_{N-2}^{[\alpha\beta\gamma]}$$
$$+\frac{\chi_N^{[\alpha]}}{v_\alpha}\left(\langle\phi_N^{[\alpha]}|H|\phi_N^{[\alpha]}\rangle-\overline{E}\right)\Bigg] \tag{32a}$$

$$=\frac{2N^2}{\chi_N}\Bigg[\sum_{\beta\in\Theta}^{P_\beta\neq P_\alpha}G_{\alpha\beta}v_\beta\chi_{N-1}^{[\alpha\beta]}$$
$$+(N-1)^2\sum_{\beta,\gamma\in\Theta}^{\boldsymbol{dif}\,\alpha\beta\gamma}G_{\alpha\beta,\gamma}v_\beta(v_\gamma)^2\chi_{N-2}^{[\alpha\beta\gamma]}$$
$$+v_\alpha\chi_{N-1}^{[\alpha]}\left(d_\alpha+f_\alpha+\langle\phi_{N-1}^{[\alpha]}|H|\phi_{N-1}^{[\alpha]}\rangle-\overline{E}\right)\Bigg]. \tag{32b}$$

The gradient of $\overline{E}$ is perpendicular to $\vec{v}$ because the overall norm of v_α does not affect $\overline{E}$, which is

$$\nabla\overline{E}\cdot\vec{v}=\sum_{\alpha\in\Theta}v_\alpha\frac{\partial\overline{E}}{\partial v_\alpha}=0.$$

This identity is used for checking codes.

The three-body part of the HF single-particle energy is as follows:

$$e_\alpha^{(3)}=\frac{1}{2}\sum_{\beta,\gamma\in\mathrm{SD}}V_{\alpha\beta\gamma\gamma\beta\alpha}$$
$$=\sum_{\beta\in\mathrm{SD}}\left(\delta_\alpha V_{\alpha\beta\tilde{\alpha}\tilde{\alpha}\beta\alpha}+\frac{1}{2}V_{\alpha\beta\tilde{\beta}\tilde{\beta}\beta\alpha}\right)+\frac{1}{2}\sum_{\beta,\gamma\in\mathrm{SD}}^{\boldsymbol{dif}\,\alpha\beta\gamma}V_{\alpha\beta\gamma\gamma\beta\alpha}$$
$$=\delta_\alpha\sum_{\substack{\beta\in\Theta\\ \beta\in\mathrm{SD}}}G_{\alpha\alpha,\beta}+\frac{1}{2}\sum_{\substack{\beta\in\Theta\\ \beta\in\mathrm{SD}}}G_{\beta\beta,\alpha}+\frac{1}{2}\sum_{\substack{\beta,\gamma\in\Theta\\ \beta,\gamma\in\mathrm{SD}}}^{\boldsymbol{dif}\,\alpha\beta\gamma}F_{\alpha\beta\gamma}$$
$$=\frac{1}{2}\sum_{\beta,\gamma\in\Theta}^{\beta,\gamma\in\mathrm{SD}}F_{\alpha\beta\gamma}, \tag{33}$$

where $\beta\in\mathrm{SD}$ means the β orbit occupied in the HF Slater determinant ($n_\beta=1$), and

$$\delta_\alpha=\begin{cases}1, & \text{if } \alpha\in\mathrm{SD},\\ 0, & \text{else.}\end{cases}$$

The HF single-particle energy, which includes three-body forces, is

$$e_\alpha = \epsilon_{\alpha\alpha} + \sum_{\beta\in\Theta}^{\beta\in\mathrm{SD}} \Lambda_{\alpha\beta} + \frac{1}{2}\sum_{\beta,\gamma\in\Theta}^{\beta,\gamma\in\mathrm{SD}} F_{\alpha\beta\gamma}. \tag{34}$$

The Fermi energy $e_F \equiv (e_{h.o.} + e_{l.e.})/2$, where $e_{h.o.}$ and $e_{l.e.}$ are the HF single-particle energy e_α of the highest occupied orbit and lowest empty orbit. If n_α(11) is set to 1 for occupied orbits and 0 for empty orbits, which is equivalent to setting v_α (3) to a very large number and 0, respectively, the pair condensate (1) reduces to the HF Slater determinant. In this case, $f_\alpha \approx 2e_\alpha^{(3)}$, where $e_\alpha^{(3)}$ is the three-body part of the HF single-particle energy e_α.

At energy minimum, the gradients given by (32a) and (32b) vanish, which implies

$$v_\alpha = \frac{\langle\phi_N^{[\alpha]}|H|\phi_N^{[\alpha]}\rangle - \overline{E}}{-N^2 A_\alpha/\chi_N^{[\alpha]}} \tag{35a}$$

$$= \frac{-A_\alpha/\chi_{N-1}^{[\alpha]}}{d_\alpha + f_\alpha + \langle\phi_{N-1}^{[\alpha]}|H|\phi_{N-1}^{[\alpha]}\rangle - \overline{E}}, \tag{35b}$$

where

$$A_\alpha = \sum_{\beta\in\Theta}^{P_\beta\neq P_\alpha} G_{\alpha\beta} v_\beta \chi_{N-1}^{[\alpha\beta]} + (N-1)^2 \sum_{\beta,\gamma\in\Theta}^{\boldsymbol{dif}\,\alpha\beta\gamma} G_{\alpha\beta,\gamma} v_\beta (v_\gamma)^2 \chi_{N-2}^{[\alpha\beta\gamma]}. \tag{36}$$

Numerically, (35a) is usually chosen when $e_\alpha \ll e_F$ (here $\ll$ means that the α orbit is well below the Fermi surface), and (35b) is usually selected when $e_\alpha \gg e_F$. When $e_\alpha \ll e_F$, physical arguments imply $\langle\phi_N^{[\alpha]}|H|\phi_N^{[\alpha]}\rangle - \overline{E} \approx 2(e_F - e_\alpha)$ and $d_\alpha + f_\alpha + \langle\phi_{N-1}^{[\alpha]}|\hat{W}|\phi_{N-1}^{[\alpha]}\rangle - \overline{W} \approx 0$. To avoid the numerical sign problem resulting from the subtraction of two very close numbers, (35a) is chosen. When $e_\alpha \gg e_F$, physical arguments imply $\langle\phi_N^{[\alpha]}|H|\phi_N^{[\alpha]}\rangle - \overline{E} \approx 0$ and $d_\alpha + f_\alpha + \langle\phi_{N-1}^{[\alpha]}|\hat{W}|\phi_{N-1}^{[\alpha]}\rangle - \overline{W} \approx 2(e_\alpha - e_F)$, so (35b) is selected.

The asymptotic behavior of v_α away from (above or below) the Fermi surface is also implied by the foregoing analysis,

$$v_\alpha \approx \begin{cases} \dfrac{2(e_F - e_\alpha)}{-N^2 A_\alpha/\chi_N^{[\alpha]}}, & \text{if } e_\alpha \ll e_F, \quad (37a) \\ \dfrac{-A_\alpha/\chi_{N-1}^{[\alpha]}}{2(e_\alpha - e_F)}, & \text{if } e_\alpha \gg e_F. \quad (37b) \end{cases}$$

For a physical explanation, equivalent expressions to Eq. (35a) and (35b) can be derived in terms of occupation numbers:

$$v_\alpha = \frac{\langle\phi_N^{[\alpha]}|H|\phi_N^{[\alpha]}\rangle - \overline{E}}{-B_\alpha} \tag{38a}$$

$$= \frac{-C_\alpha}{d_\alpha + f_\alpha + \langle\phi_{N-1}^{[\alpha]}|H|\phi_{N-1}^{[\alpha]}\rangle - \overline{E}}, \tag{38b}$$

where

$$B_\alpha = \sum_{\beta\in\Theta}^{P_\alpha\neq P_\beta} G_{\alpha\beta} \frac{1}{v_\beta} \langle\phi_N^{[\alpha]}|\hat{n}_\beta|\phi_N^{[\alpha]}\rangle + \sum_{\beta,\gamma\in\Theta}^{\boldsymbol{dif}\,\alpha\beta\gamma} G_{\alpha\beta,\gamma} \frac{1}{v_\beta} \langle\phi_N^{[\alpha]}|\hat{n}_\beta|\phi_N^{[\alpha]}\rangle\langle\phi_{N-1}^{[\alpha\beta]}|\hat{n}_\gamma|\phi_{N-1}^{[\alpha\beta]}\rangle, \tag{39}$$

$$C_\alpha = \sum_{\beta\in\Theta}^{P_\alpha\neq P_\beta} G_{\alpha\beta} v_\beta (1 - \langle\phi_{N-1}^{[\alpha]}|\hat{n}_\beta|\phi_{N-1}^{[\alpha]}\rangle) + \sum_{\beta,\gamma\in\Theta}^{\boldsymbol{dif}\,\alpha\beta\gamma} G_{\alpha\beta,\gamma} v_\beta (1 - \langle\phi_{N-1}^{[\alpha]}|\hat{n}_\beta|\phi_{N-1}^{[\alpha]}\rangle)\langle\phi_{N-1}^{[\alpha\beta]}|\hat{n}_\gamma|\phi_{N-1}^{[\alpha\beta]}\rangle, \tag{40}$$

and equivalent expressions to Eq. (37a) and (37b) can also be derived in terms of occupation numbers:

$$v_\alpha \approx \begin{cases} \dfrac{2(e_F - e_\alpha)}{-B_\alpha}, & \text{if } e_\alpha \ll e_F, \quad (41a) \\ \dfrac{-C_\alpha}{2(e_\alpha - e_F)}, & \text{if } e_\alpha \gg e_F. \quad (41b) \end{cases}$$

The exact [Eqs. (35a) and (35b)] and asymptotic [Eqs. (37a) and (37b)] expressions for v_α are used to minimize the energy in the algorithm.

V. COMPUTER ALGORITHM

In Sec. II, $|\phi_N\rangle$ was expressed using v_α (Eqs. (1) and (3)). In Sec. III, normalizations were expressed using v_α (Eqs. (8), (9), and (10)) and the average energy $\overline{E}$ (24) was expressed using normalizations and v_α. In Sec. IV, we presented the gradient of energy expressed by v_α (Eqs. (32a) and (32b)) and the expression of v_α when the gradient equals zero (Eqs. (35a) and (35b)). We also derived the asymptotic expression of v_α when the α orbit away from (above or below) the Fermi surface and the gradient equal zero (Eqs. (37a) and (37b)).

Ultimately, the objetive is to minimize the average energy $\overline{E}$ to arbitrary precision using these equations. The initial value of v_α is inconsequential because all initial $\vec{v}$ will converge to the same final $\vec{v}$ that minimize the energy. The Euclidean norm of $\vec{v}$ does not affect $\overline{E}$, so the degrees of freedom of $\vec{v}$ are $\Omega - 1$(the dimension of the single-particle space is $D = 2\Omega$, where Ω is the number of vacancies for Kramers pairs). In practice, when using ma-

chine precision, the largest dimension of the single-particle space D is approximately 40, for which the numerical sign problem will not occur. Considering the limitations of CPU and memory in laptops, 120 effective digits were set in this study (using *Mathematica* function *SetPrecision [120]*), and $D=2\Omega=240$ was set for the model space to compute the final $\overline{E}$. The complete algorithm includes three consecutive steps:

Step 1. Sort the single-particle basis states $|\alpha\rangle$ by their HF energy e_α (35) and occupy the lowest $2N$ basis states. Given that this study is VDPC+BCS rather than VDPC+HFB, the HF equation was solved without mixing the basis states. This step is not needed if the input single-particle basis is already the HF basis.

Step 2. Select, around e_F, the first single-particle valence space (VS1) of dimension $D=2\Omega=40$ (20 above the Fermi surface and 20 below the Fermi surface, so the number of particles $2N=20$). This model space is half-filled. The single-particle basis states below VS1 are totally filled, forming an inert core that effectively corrects the VS1 single-particle energy using its HF mean field. Within VS1, the *MATLAB* function *fminunc* was used to find the minimum of the unconstrained multivariable function to minimize $\overline{E}$. The resultant v_α of VS1 is called $v_\alpha^{(1)}$. Step 2 only uses double precision.

Step 3. Select, around e_F, the second valence space (VS2) of dimension $D=2\Omega=240$. If $|\alpha\rangle$ belongs to VS1, initialize v_α of VS2 to be$v_\alpha^{(1)}$. Otherwise, if $e_\alpha<e_F$ ($e_\alpha>e_F$), initialize v_α of VS2 to be a very large (small) number so that $n_\alpha\approx 1$ ($n_\alpha\approx 0$). The analytical formulas (35a) and (35b) allows iterating on v_α until the average energy $\overline{E}$ converges to a desired precision (more iterations provide more precision; usually 10 iterations suffice). The resultant v_α of VS2 is the final result, which finishes the algorithm. Step 3 uses a 120 precision to compute normalizations [according to Eqs. (8)–(10)] and $\overline{E}$ [Eq. (24)] to overcome the sign problem, and double precision to compute $\partial\overline{E}/\partial v_\alpha$ [according to Eqs. (32a) and (32b)] and v_α [Eqs. (35a) and (35b)], which will not give rise to the sign problem, because Eqs. (8)–(10) lose relatively more precision.

VI. A SEMIREALISTIC EXAMPLE

In this section, we demonstrate the algorithm in a semirealistic example of the rare-earth nucleus $^{158}_{64}$Gd, considering only the neutron degree of freedom ($2N=94$). The single-particle levels are Nilsson levels (at quadrupole deformation $\beta=0.349$, which is the experimental value). The two-body interaction is the low-momentum NN interaction $V_{\mathrm{low-k}}$, which is derived from the free-space N^{3}LO potential [76].

The program published by Hjorth-Jensen [77] was used to calculate (in the absence of Coulomb, charge symmetry breaking, or charge-independent breaking) the two-body matrix elements of $V_{\mathrm{low-k}}$ in the spherical harmonic oscillator basis up to (and including) the $\mathcal{N}=14$ major shell with a standard momentum cutoff 2.1 fm^{-1} ($\mathcal{N}=2n_r+l$ is the major-shell quantum number). The Nilsson model is then diagonalized on this spherical $\mathcal{N}\leqslant 14$ basis, and the eigenenergies $\epsilon_{\alpha\alpha}$ and eigen wave functions transform the spherical two-body matrix elements into matrix elements on the Nilsson basis, as used in the Hamiltonian (15).

This example is comprehensively covered in the original VDPC+BCS algorithm [1]. Let us further discuss the three-body interaction. Random $G_{\alpha\beta,\gamma}$ and $F_{\alpha\beta\gamma}$ matrices were employed; the formulas provided next describe how the $G_{\alpha\beta,\gamma}$ and $F_{\alpha\beta\gamma}$ matrices are generated. The $G_{\alpha\beta,\gamma}$ matrix is generated from the $G_{\alpha\beta}$ matrix, and $G_{\alpha\beta,\gamma}=coef\times[G_{\alpha\beta}+err\times rand\times mean(G_{\alpha\beta})]$, where "coef" is an adjustable three-body strength and "err" is the degree of dispersion. The function *rand* provides a single uniformly distributed random number in the interval $(-0.5,0.5)$ and $mean(G_{\alpha\beta})$ computes the mean over all elements of the $G_{\alpha\beta}$ matrix. Similarly, the $F_{\alpha\beta\gamma}$ matrix is generated from the $\Lambda_{\alpha\beta}$ matrix, and $F_{\alpha\beta\gamma}=coef\times[\Lambda_{\alpha\beta}+err\times rand\times mean(\Lambda_{\alpha\beta})]$. Note that $G_{\alpha\beta,\gamma}=G_{\beta\alpha,\gamma}$, $F_{\alpha\beta\gamma}=F_{\mathcal{P}\{\alpha\beta\gamma\}}$, $G_{\alpha\alpha,\gamma}=F_{\alpha\alpha\gamma}$, and $G_{\alpha\beta,\alpha}=G_{\alpha\beta,\beta}=F_{\alpha\alpha\alpha}=0$. Therefore, not all elements of the $G_{\alpha\beta,\gamma}$ and $F_{\alpha\beta\gamma}$ matrices are independent; only some independent elements are generated, and consequently non-independent elements are also automatically generated. The three-body strength was set to 0.01 and the degree of dispersion to 1 to make the total three-body part of average energy $\overline{W}$ equal to -154.09 MeV, which is approximately 0.2 times as large as the total two-body part of average energy $\overline{V}$, which is

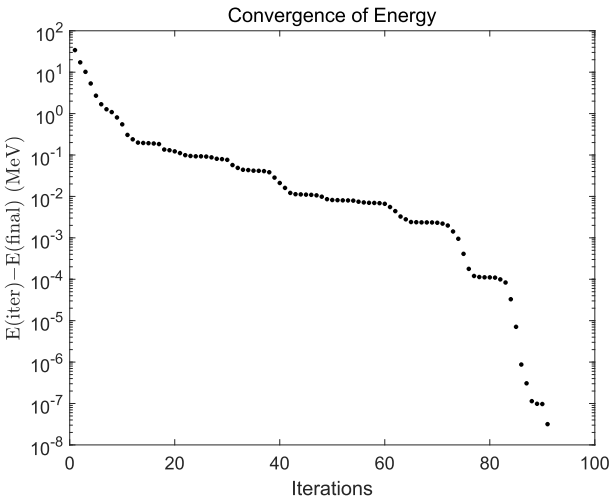

Fig. 1. Convergence of energy in Step 2 using double precision. The horizontal axis represents the number of iterations. The vertical axis shows the energy at each iteration E(iter), relative to the final converged energy E(final). The total time cost of all iterations was 2.118 s using a laptop (Intel Core i7-8550U @ 1.80 GHz, 32.0 GB RAM, no parallel computing).

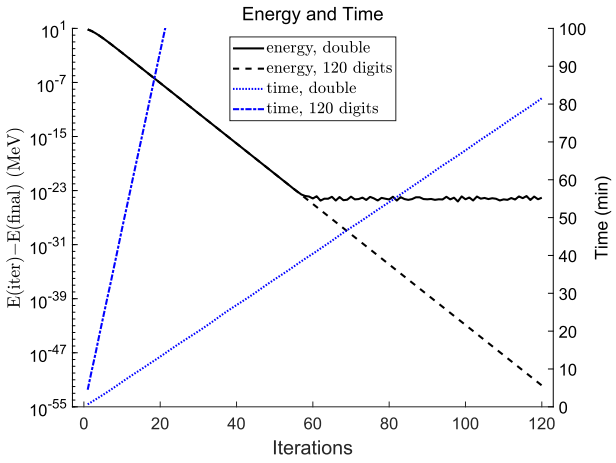

Fig. 2. (color online) Energy and time using two types of precision: double and 120 effective digits. The solid and dashed lines correspond to the left vertical axis and show the energy at each iteration E(iter), relative to the final converged energy E(final). The dotted and dash-dot lines correspond to the right vertical axis, showing the accumulated computer time cost after each iteration.

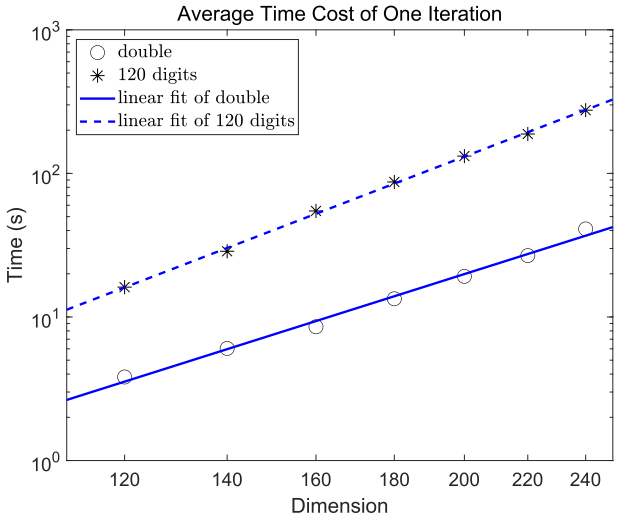

Fig. 3. (color online) Average computing time cost of one iteration in different model spaces. The horizontal axis represents the dimension of each model space, whereas the vertical axis represents the time cost of one iteration (averaged over 20 iterations). The circle symbols represent iterations using double precision, while the asterisk symbols represent iterations using 120 effective digits. The solid and dashed lines represent their linear fits, respectively.

equal to −911.93 MeV. The $G_{\alpha\beta,\gamma}$ and $F_{\alpha\beta\gamma}$ matrices also satisfy the trend that the absolute values of the matrix elements are larger when the α and β orbits are closer.

Figure 1 shows how $\overline{E}$ converges in Step 2 as the number of iteration increases. The dimension of the model in this case was $D = 2\Omega = 40$ (20 above the Fermi surface and 20 below the Fermi surface), as previously explained. The energy error decreases on the semi-log plot. After approximately 90 iterations, the error was less than 10^{-7} MeV. The total time cost of all iterations was 2.118 s using double precision.

Figure 2 shows how $\overline{E}$ converges in Step 3. The lowest 240 single-particle orbits (94 below the Fermi surface and $240-94=146$ above the Fermi surface) were selected, considering that the level density in the upper layer is relatively small. Therefore, the number of single-particle orbits above the Fermi surface was slightly larger. Its dimension $D = 2\Omega = 240$ was the largest dimension set in this study because of the limited computing resources available. The computer code was run twice using double precision and 120 precision, respectively. The legend "120 digits" denotes the use of 120 precision everywhere, whereas the legend "double" denotes the use of 120 effective digits only when necessary (to overcome the sign problem), switching to double precision for higher speed. Comparing these two executions, "120 digits" was significantly slower than "double", but it converged to higher precision.

In practical terms, the energy $\overline{E}$ can be minimized to any arbitrary precision. The energy error decreased linearly on the semi-log plot for the "120 digits" execution, as shown in Fig. 2, so $\overline{E}$ converged exponentially with the number of iterations. After 120 iterations, the error was less than 10^{-50} MeV. It is not difficult to conclude that if the precision used in Step 3 (greater than 120) is increased and more iterations are carried out, the precision of the convergent energy will increase as well. For the "double" execution, the best precision achievable was approximately 10^{-23} MeV, reached near the 55th iteration. This execution produced the same result as that of the "120 digits" execution until this point (the two energy curves are indistinguishable). After this point, the precision of the "double" execution fluctuated and no improvement was achieved. To summarize, the "double" execution is preferred because it runs much faster and the precision of 10^{-23} MeV is sufficient in nuclear physics.

The cost of computing time per iteration is primarily determined by the dimension of the single-particle model space. For the "double" run, $T \approx (D/82.5)^{3.38}$, as shown in Fig. 3, where T is the average time of one iteration (averaged over 20 iterations) in unit of second and $D = 2\Omega$ is the dimension. For the "120 digits" run, $T \approx (D/61.0)^{4.11}$. All the numerical computations were completed on a laptop having a one quad-core CPU (Intel Core i7-8550U @ 1.80 GHz), dual 16.0 GB memory (32.0 GB in total, operating at 2400 MHz). A single core was employed in all computations (i.e., no parallel computing was set). All the time costs given in the text or plotted in the figures represent actual time costs on this laptop.

A complete execution is shown in Fig. 4. The exact energy E(exact) is the energy after 120 iterations using random three-body forces with 120 precision when the dimension is equal to 240 (the maximum dimension,

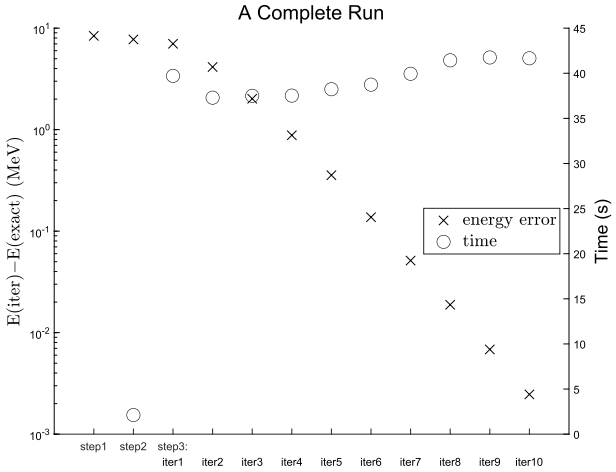

Fig. 4. Energy and time in a complete run. The horizontal axis represents the three steps listed in Sec. V, where Step 3 is divided into 10 iterations. The cross symbols correspond to the left axis and show the energy error after each step or iteration, relative to the exact energy E(exact) (converged energy in $D = 240$ model space). The circle symbols correspond to the right axis and show the time cost spent by each step or iteration, in unit of second.

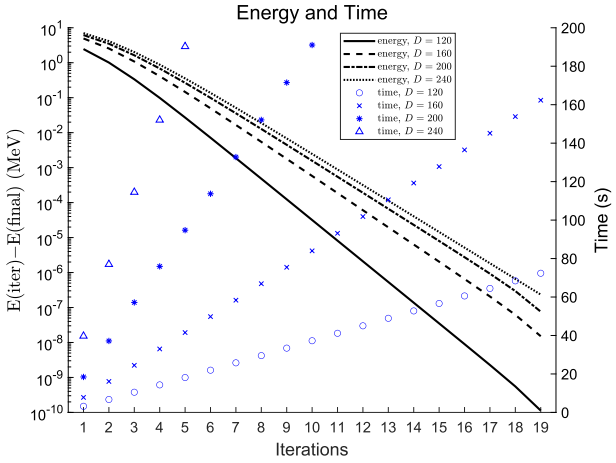

Fig. 5. (color online) Energy and time in different model spaces. The solid, dashed, dash-dot, and dotted lines correspond to the left vertical axis, and show the energy errors. The circle, cross, asterisk, and triangle symbols correspond to the right vertical axis, and show the accumulated time cost after each iteration.

maximum precision, and maximum number of iterations employed in a single program execution in this study). This energy is the smallest energy considered in this work; it is more precise than 10^{-50} MeV (see Fig. 2) and is regarded as the physically real energy of this system. Step 1 was HF and incurred negligible time. The energy error after step 2 was approximately 8 MeV, which means that the VS1 energy minimum was higher than the VS2 energy minimum by approximately 8 MeV (the dimension of VS1 was $D = 40$ whereas that of VS2 was

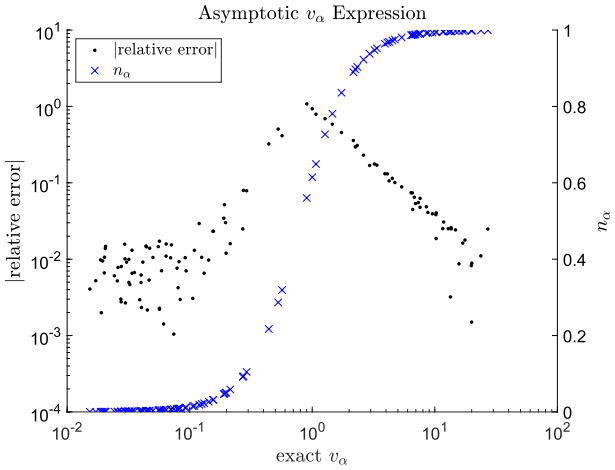

Fig. 6. (color online) Error of the asymptotic v_α as a function of the exact value of v_α. The relative error is given by $RE \equiv (v_\alpha^{\text{asymptotic}}/v_\alpha^{\text{exact}}) - 1$. The horizontal axis represents the exact v_α. The dot symbols correspond to the left vertical axis and show $|RE|$. The cross symbols correspond to the right vertical axis and represent the exact occupation number n_α.

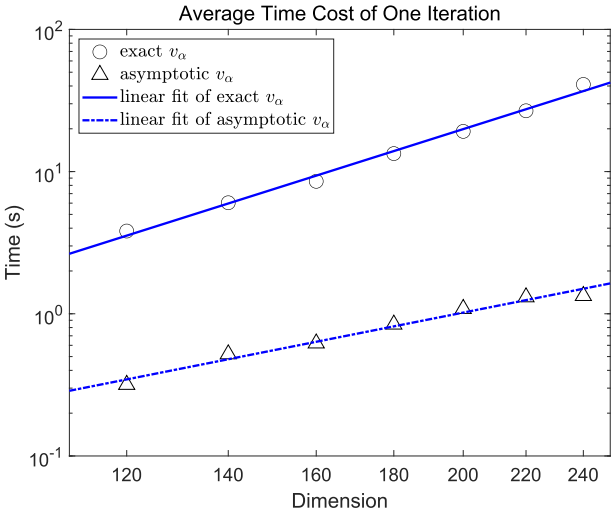

Fig. 7. (color online) Average computing time cost of one iteration in different model spaces. The horizontal axis represents the dimension of each model space, whereas the vertical axis represents the time cost of one iteration (averaged over 20 iterations). The circle symbols represent iterations according to the exact v_α expressions (35a) and (35b), while the triangle symbols represent iterations according to the asymptotic v_α expressions (37a) and (37b). The solid and dash-dot lines represent their linear fit, respectively.

$D = 240$), because the randomly generated $G_{\alpha\beta,\gamma}$ and $F_{\alpha\beta\gamma}$ did not decrease as $|e_\gamma - e_\alpha|$ (or $|e_\gamma - e_\beta|$) increased. After the three steps, the energy error was reduced to approximately 2 keV in less than 7 min. Figure 5 plots the energy convergence pattern in different model spaces. The energy error curves are linear on a semi-log plot, so the energy converges exponentially with increasing number

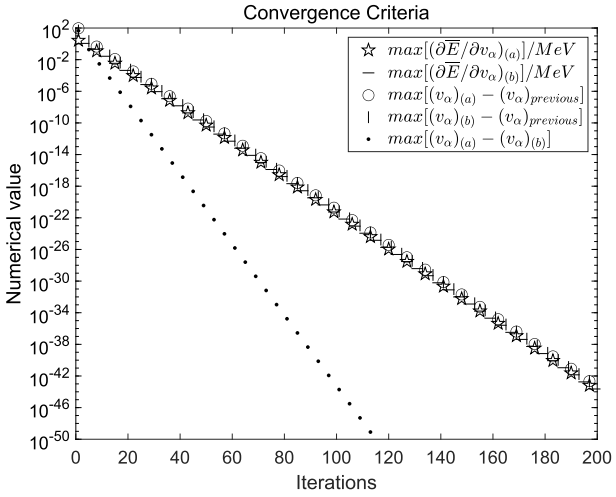

Fig. 8. Partial convergence criteria in one program execution. The horizontal axis represents the number of iterations whereas the vertical axis represents the numerical value of each expression. The pentagram and horizontal line symbols represent the maximum numerical values of (32a) and (32b), respectively. The circle (vertical line) symbols represent the maximum numerical value of the difference between (35a) and (35b) in the current iteration and exact v_α in the previous iteration. The point symbols represent the maximum numerical value of the difference between (35a) and (35b).

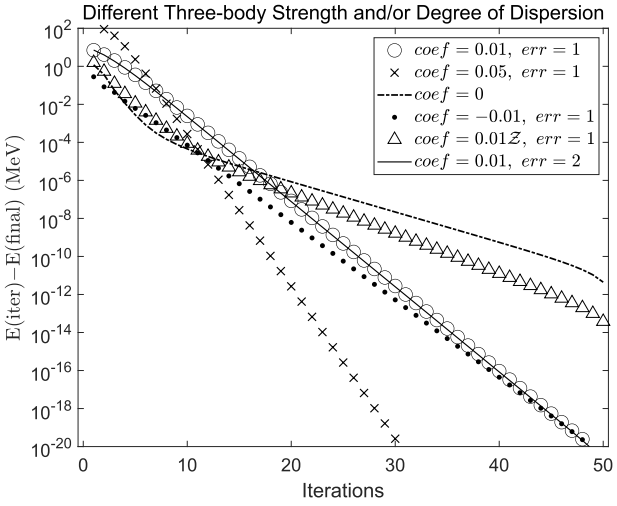

Fig. 9. Convergence of energy using different three-body Hamiltonians in the $D = 240$ model space. The six curves correspond to six executions using different three-body strength $coef$ and/or degree of dispersion err. For each execution, its curve shows the energy at every iteration E(iter), relative to the final converged energy E(final) in this execution. $\mathcal{Z}$ is a coefficient whose value ranges between 0.1 and 1 and decreases sharply as γ moves away from α and β.

of iterations. As the dimension of model space increased, the rate of convergence did not slow down significantly. For a specified dimension, the cumulative time cost increased linearly with the number of iterations. Therefore, the time cost was approximately the same for each iteration. Note also that increasing the dimension of the model space by 40 approximately doubles the time cost of a single iteration.

The asymptotic expressions (37a) and (37b) faithfully reproduce the exact values of v_α (35a) and (35b) away from the Fermi surface. Figure 6 compares them at the energy minimum in the $D = 240$ model space. Near the Fermi surface (i.e., the vicinity of $v_\alpha = 1$), the asymptotic expressions (37a) and (37b) are not applicable, so the largest absolute value of relative error $|RE| \approx 1$ appears here. Going away from the Fermi surface, $|RE|$ becomes gradually smaller. Of these 120 different values of v_α, 82.5% have $|RE| < 10\%$ and 36.7% have $|RE| < 1\%$. Figure 7 shows that the average computing time cost per one iteration of both exact v_α and asymptotic v_α increases approximately linearly with the dimension on the log-log plot. For the exact v_α run, the circle symbols and solid line are exactly the same as the ones for the "double" run displayed in Fig. 3, so $T \approx (D/82.5)^{3.38}$. For the asymptotic v_α run, $T \approx (D/198)^{2.12}$; it was a much faster execution.

Figure 8 illustrates a portion of the convergence criteria in this program, using 120 precision and $D = 240$ model space. After convergence, all five criteria in the figure should be equal to zero. Here "equal to zero" means a non-specific, acceptable error. It can be seen that all five criteria decreased linearly in the semi-log plot as the number of iterations increased. After 20 iterations, all the convergence criteria were reduced by at least four orders of magnitude. There are three additional criteria not shown in the figure; $\max[(\partial\overline{E}/\partial v_\alpha)_{(a)} - (\partial\overline{E}/\partial v_\alpha)_{(b)}]$, $\sum_{\alpha\in\Theta} v_\alpha(\partial\overline{E}/\partial v_\alpha)_{(a)}$, and $\sum_{\alpha\in\Theta} v_\alpha(\partial\overline{E}/\partial v_\alpha)_{(b)}$ are always zero during 200 iterations, which further proves that the energy truly converges.

We ran the extended VDPC+BCS code six times, each running through the first and second steps. The second step was iterated 51 times. These six times used different three-body strength and/or degree of dispersion, as shown in Fig. 9. The dash-dotted line $coef = 0$ corresponds to no three-body interaction, only one-body, and two-body interactions. The values represented by the circle symbol are used in all previous figures and are also described in the first paragraph of this section. It can be seen from the figure that after the three-body force is added, the energy converges faster, and when other conditions remain unchanged, the greater the three-body strength, the faster the energy convergence, and the positive or negative nature of the three-body force will not affect the convergence speed. By comparing the solid line and circle symbol, we can conclude that the degree of dispersion does not affect the convergence speed. The triangle symbol means that after a more realistic simulation of the three-body force (the three-body force matrix ele-

ments rapidly become smaller as α, β, and γ get away from each other), the energy convergence curve will be closer to the curve of only one-body and two-body interactions, but it will converge faster, and the accuracy will be higher after the same number of iterations. By using different random three-body force matrices $G_{\alpha\beta,\gamma}$ and $F_{\alpha\beta\gamma}$, it is shown that the three-body force is correctly added in this study, regardless of the three-body force used, and including the real three-body force. Indeed, it can be correct and quickly converge to any arbitrary precision.

VII. CONCLUSIONS

This study extends the VDPC+BCS formalism by including three-body forces. In particular, the average energy and its gradient are derived for a three-body Hamiltonian in terms of the coherent-pair structure v_α. The gradient is vanished to obtain the analytical expression of v_α at the energy minimum. The extended VDPC+BCS algorithm iterates on these v_α expressions to minimize the average energy for a three-body Hamiltonian, until arbitrary precision. Asymptotic expressions of v_α away from (above or below) the Fermi surface are also provided. They are highly accurate, as shown in Fig. 6, and can be numerically evaluated quickly, as shown in Fig. 7.

The new code is demonstrated using a numerical example with realistic two-body and random three-body forces in large model spaces. Figure 4 shows a complete numerical example execution. In the given model space, the average energy $\overline{E}$ can be minimized to any arbitrary precision, as shown in Fig. 2. The pattern of energy convergence and real computer time cost are presented in Fig. 5. The numerical sign problem emerges in some areas of the code if double-precision floating-point numbers are used globally. In these parts, higher precision (120 effective digits) was employed to solve this issue. Numerical expressions of the computing time cost per iteration are also provided using the dimension of the single-particle model space, as shown in Fig. 3. The new code is published together with this manuscript.

In the future, realistic three-body forces will be employed to study their effect on the coherent-pair condensate. Possible changes of various pairing phenomena will also be studied.

ACKNOWLEDGMENTS

The author gratefully acknowledges discussions with Prof. L. Y. Jia.

References

[1] L. Y. Jia, Phys. Rev. C **99**, 014302 (2019)
[2] L. Jia, Computer Physics Communications **248**, 106967 (2020)
[3] B. S. Pudliner, V. R. Pandharipande, J. Carlson *et al.*, Phys. Rev. Lett. **74**, 4396 (1995)
[4] B. S. Pudliner, V. R. Pandharipande, J. Carlson *et al.*, Phys. Rev. C **56**, 1720 (1997)
[5] J. Carlson and R. Schiavilla, Rev. Mod. Phys. **70**, 743 (1998)
[6] S. C. Pieper, R. B. Wiringa, and J. Carlson, Phys. Rev. C **70**, 054325 (2004)
[7] W. Zuo, I. Bombaci, and U. Lombardo, Eur. Phys. J. A **50**, 12 (2014)
[8] S. R. Stroberg, H. Hergert, S. K. Bogner *et al.*, Annu. Rev. Nucl. Part. S. **69**, 307 (2019)
[9] I. Bombaci and U. Lombardo, Phys. Rev. C **44**, 1892 (1991)
[10] W. Zuo, I. Bombaci, and U. Lombardo, Phys. Rev. C **60**, 024605 (1999)
[11] W. Zuo, A. Lejeune, U. Lombardo *et al.*, Eur. Phys. J. A - Hadrons and Nuclei **14**, 469 (2002)
[12] W. Zuo, L. G. Cao, B. A. Li *et al.*, Phys. Rev. C **72**, 014005 (2005)
[13] W. Zuo, U. Lombardo, H.-J. Schulze *et al.*, Phys. Rev. C **74**, 014317 (2006)
[14] I. Vidaña, C. Providência, A. Polls *et al.*, Phys. Rev. C **80**, 045806 (2009)
[15] I. Vidaña, A. Polls, and C. Providência, Phys. Rev. C **84**, 062801 (2011)
[16] H. Huber, F. Weber, and M. K. Weigel, Phys. Rev. C **51**, 1790 (1995)
[17] C.-H. Lee, T. T. S. Kuo, G. Q. Li *et al.*, Phys. Rev. C **57**, 3488 (1998)
[18] E. van Dalen, C. Fuchs, and A. Faessler, Nucl. Phys. A **744**, 227 (2004)
[19] E. N. E. v. Dalen, C. Fuchs, and A. Faessler, Phys. Rev. C **72**, 065803 (2005)
[20] E. N. E. van Dalen, C. Fuchs, and A. Faessler, Phys. Rev. Lett. **95**, 022302 (2005)
[21] Z.-Y. Ma, J. Rong, B.-Q. Chen *et al.*, Phys. Lett. B **604**, 170 (2004)
[22] F. Sammarruca and P. Krastev, Phys. Rev. C **73**, 014001 (2006)
[23] T. Klähn, D. Blaschke, S. Typel *et al.*, Phys. Rev. C **74**, 035802 (2006)
[24] T. Frick, H. Müther, A. Rios *et al.*, Phys. Rev. C **71**, 014313 (2005)
[25] K. Gad and K. Hassaneen, Nucl. Phys. A **793**, 67 (2007)
[26] A. Rios, A. Polls, and W. H. Dickhoff, Phys. Rev. C **79**, 064308 (2009)
[27] A. Rios and V. Somà, Phys. Rev. Lett. **108**, 012501 (2012)
[28] P. Bożek and P. Czerski, Eur. Phys. J. A - Hadrons and Nuclei **11**, 271 (2001)
[29] P. Bożek, Eur. Phys. J. A - Hadrons and Nuclei **15**, 325 (2002)
[30] P. Bożek, Phys. Rev. C **65**, 054306 (2002)
[31] V. Somà and P. Bożek, Phys. Rev. C **78**, 054003 (2008)
[32] V. Somà and P. Bożek, Phys. Rev. C **80**, 025803 (2009)
[33] Y. Dewulf, D. Van Neck, and M. Waroquier, Phys. Lett. B **510**, 89 (2001)
[34] Y. Dewulf, D. Van Neck, and M. Waroquier, Phys. Rev. C **65**, 054316 (2002)

[35] Y. Dewulf, W. H. Dickhoff, D. Van Neck *et al*., Phys. Rev. Lett. **90**, 152501 (2003)
[36] R. B. Wiringa, V. Fiks, and A. Fabrocini, Phys. Rev. C **38**, 1010 (1988)
[37] A. Akmal, V. R. Pandharipande, and D. G. Ravenhall, Phys. Rev. C **58**, 1804 (1998)
[38] G. H. Bordbar and M. Modarres, Phys. Rev. C **57**, 714 (1998)
[39] M. Modarres and G. H. Bordbar, Phys. Rev. C **58**, 2781 (1998)
[40] G. H. Bordbar and M. Bigdeli, Phys. Rev. C **75**, 045804 (2007)
[41] G. H. Bordbar and M. Bigdeli, Phys. Rev. C **77**, 015805 (2008)
[42] A. E. L. Dieperink, Y. Dewulf, D. Van Neck *et al*., Phys. Rev. C **68**, 064307 (2003)
[43] Z. H. Li, U. Lombardo, H.-J. Schulze *et al*., Phys. Rev. C **74**, 047304 (2006)
[44] P. Gögelein, E. N. E. van Dalen, K. Gad *et al*., Phys. Rev. C **79**, 024308 (2009)
[45] N. Onishi and J. Negele, Nucl. Phys. A **301**, 336 (1978)
[46] L. Coraggio, J. W. Holt, N. Itaco *et al*., Phys. Rev. C **89**, 044321 (2014)
[47] R. Rajaraman and H. A. Bethe, Rev. Mod. Phys. **39**, 745 (1967)
[48] M. Heinz, A. Tichai, J. Hoppe *et al*., Phys. Rev. C **103**, 044318 (2021)
[49] J. Hoppe, A. Tichai, M. Heinz *et al*., Phys. Rev. C **103**, 014321 (2021)
[50] O. Benhar, A. Fabrocini, and S. Fantoni, Nucl. Phys. A **505**, 267 (1989)
[51] O. Benhar, A. Fabrocini, and S. Fantoni, Nucl. Phys. A **550**, 201 (1992)
[52] M. Baldo and F. Burgio, *Microscopic theory of the nuclear equation of state and neutron star structure*, in *Physics of Neutron Star Interiors*, edited by D. Blaschke, A. Sedrakian, and N. K. Glendenning (Springer Berlin Heidelberg, Berlin, Heidelberg, 2001) pp. 1–29.
[53] M. Baldo, *Nuclear methods and the nuclear equation of state* (World Scientific, 1999).
[54] M. Baldo and C. Maieron, J. Phys. G : Nucl.Part. Phys. **34**, R243 (2007)
[55] K. Dietrich, H. J. Mang, and J. H. Pradal, Phys. Rev. **135**, B22 (1964))
[56] J. Dukelsky and G. Sierra, Phys. Rev. B **61**, 12302 (2000)
[57] G. G. Dussel, S. Pittel, J. Dukelsky *et al*., Phys. Rev. C **76**, 011302 (2007)
[58] N. Sandulescu and G. F. Bertsch, Phys. Rev. C **78**, 064318 (2008)
[59] Y. X. Yu, Y. Lu, G. J. Fu *et al*., Phys. Rev. C **106**, 044309 (2022)
[60] M. Bender, P.-H. Heenen, and P.-G. Reinhard, Rev. Mod. Phys. **75**, 121 (2003)
[61] P. Ring and P. Schuck, *The nuclear many-body problem* (Springer Science & Business Media, 2004).
[62] M. Anguiano, J. Egido, and L. Robledo, Phys. Lett. B **545**, 62 (2002)
[63] J. A. Sheikh and P. Ring, Nucl. Phys.A **665**, 71 (2000)
[64] M. Anguiano, J. Egido, and L. Robledo, Nuclear Physics A **696**, 467 (2001)
[65] M. V. Stoitsov, J. Dobaczewski, R. Kirchner *et al*., Phys. Rev. C **76**, 014308 (2007)
[66] G. Hupin and D. Lacroix, Phys. Rev. C **86**, 024309 (2012)
[67] L. Y. Jia, Journal of Physics G: Nuclear and Particle Physics **42**, 115105 (2015)
[68] L. Y. Jia, Phys. Rev. C **96**, 034313 (2017)
[69] K. Allaart, E. Boeker, G. Bonsignori *et al*., Phys. Rep. **169**, 209 (1988)
[70] Y. Zhao and A. Arima, Phys. Rep. **545**, 1 (2014)
[71] L. Y. Jia and C. Qi, Phys. Rev. C **94**, 044312 (2016)
[72] C. Qi, L. Y. Jia, and G. J. Fu, Phys. Rev. C **94**, 014312 (2016)
[73] I. Talmi, *Simple models of complex nuclei: the shell model and interacting boson model* (Routledge, 2017)
[74] A. L. Goodman, *Hartree--Fock--Bogoliubov theory with applications to nuclei*, Adv. Nucl. Phys. Vol. **11** (United States, 1979)
[75] L. Y. Jia, Phys. Rev. C **88**, 044303 (2013)
[76] D. R. Entem and R. Machleidt, Phys. Rev. C **68**, 041001 (2003)
[77] M. Hjorth-Jensen, A. Hafreager, and J. E. Midtbø, Computational environment for nuclear structure, https://github.com/ManyBodyPhysics/CENS (2018)